Protocadherin-18b interacts with Nap1 to control motor axon growth and arborization in zebrafish

Sayantanee Biswas*, Michelle R. Emond, Phan Q. Duy, Le T. Hao, Christine E. Beattie, and James D. Jontes

Department of Neuroscience, Molecular, Cellular and Developmental Biology Graduate Program, Ohio State University Medical Center, Columbus, OH 43210

ABSTRACT **The proper assembly of neural circuits during development requires the precise control of axon outgrowth, guidance, and arborization. Although the protocadherin family of cell surface receptors is widely hypothesized to participate in neural circuit assembly, their specific roles in neuronal development remain largely unknown. Here we demonstrate that zebrafish *pcdh18b* is involved in regulating axon arborization in primary motoneurons. Although axon outgrowth and elongation appear normal, antisense morpholino knockdown of *pcdh18b* results in dose-dependent axon branching defects in caudal primary motoneurons. Cell transplantation experiments show that this effect is cell autonomous. Pcdh18b interacts with Nap1, a core component of the WAVE complex, through its intracellular domain, suggesting a role in the control of actin assembly. Like that of Pcdh18b, depletion of Nap1 results in reduced branching of motor axons. Time-lapse imaging and quantitative analysis of axon dynamics indicate that both Pcdh18b and Nap1 regulate axon arborization by affecting the density of filopodia along the shaft of the extending axon.**

Monitoring Editor
Paul Forscher
Yale University

Received: Aug 19, 2013
Revised: Dec 9, 2013
Accepted: Dec 19, 2013

INTRODUCTION

The outgrowth, guidance, and arborization of axons are central to the development and assembly of the mature nervous system. Although several molecular pathways underlying axon guidance have been discovered, our understanding of the range of mechanisms contributing to axonal morphogenesis remains incomplete. The protocadherins are the largest group within the cadherin superfamily of cell surface receptors. They are broadly divided into the clustered (*pcdhα*, *pcdhβ*, and *pcdhγ*) and nonclustered (Nollet *et al.*, 2000; Hulpiau and van Roy, 2009, 2011) genes. Human genetics reveals an involvement of nonclustered protocadherins in a variety of neurodevelopmental disorders (Hirano and Takeichi, 2012; Redies *et al.*, 2012), indicating that they play essential roles in neural circuit assembly. Although functional data are lacking for many of these genes, accumulating evidence suggests that protocadherins play a variety of roles in cell migration and cell motility (Kim *et al.*, 1998; Aamar and Dawid, 2008; Nakao *et al.*, 2008; Emond *et al.*, 2009; Biswas *et al.*, 2010), including axon outgrowth and guidance (Uemura *et al.*, 2007; Hasegawa *et al.*, 2008; Piper *et al.*, 2008; Katori *et al.*, 2009; Leung *et al.*, 2013). Inactivation of the *pcdhα* gene in mice disrupts the organization of both olfactory sensory axons and the axons of serotonergic neurons (Hasegawa *et al.*, 2008; Katori *et al.*, 2009). Similarly, deletion of *pcdh10* (*OL-pc*) results in defects in thalamocortical axon trajectories (Uemura *et al.*, 2007), and interference with Pcdh7 (NFPC) disrupts axon outgrowth in *Xenopus* retinal ganglion cells (Piper *et al.*, 2008; Leung *et al.*, 2013). However, the specific developmental and cellular functions of protocadherins remain unknown, as do the underlying molecular mechanisms.

The spinal cord of the embryonic zebrafish contains three identified motoneurons that are repeated in each spinal hemisegment and are invariant among embryos (Myers, 1985; Myers *et al.*, 1986; Eisen *et al.*, 1986). The stereotyped axon development and trajectories of these primary motoneurons (rostral primary, middle primary, caudal primary [CaP]) make them excellent models for studying axon guidance and morphogenesis. To investigate the cellular roles of protocadherins in neuronal development, we identified a protocadherin expressed in the primary motoneurons of zebrafish. Protocadherin-18b (*pcdh18b*) is a δ2-protocadherin, consisting of six extracellular cadherin motifs, a single-pass transmembrane domain,

This article was published online ahead of print in MBoC in Press (http://www.molbiolcell.org/cgi/doi/10.1091/mbc.E13-08-0475) on December 26, 2013.

*Present address: Department of Neuroscience, University of Wisconsin, Madison, WI 53706.

Address correspondence to: James D. Jontes (jontes.1@osu.edu).

Abbreviations used: BAC, bacterial artificial chromosome; CaP, caudal primary motoneuron; GFP, green fluorescent protein; Pcdh, protocadherin; MO, morpholino; Nap1, Nck-associated protein-1; Syp, synaptophysin; WT, wild type.

and a conserved intracellular domain (Kubota *et al.*, 2008). Using antisense morpholino oligonucleotides, we show that depletion of Pcdh18b interferes with the arborization of the CaP motor axon. In addition, Pcdh18b interacts with Nap1, an important regulator of actin dynamics. Antisense knockdown of Nap1 results in axon arborization defects that are similar to those due to loss of Pcdh18b. Multiphoton imaging of CaP axon dynamics reveals that the primary effect of depleting either Pcdh18b or Nap1 is a reduction in the number of axonal filopodia. Thus both Pcdh18b and Nap1 may contribute to the elaboration of mature axonal arbors by regulating the rate of branch initiation during development.

RESULTS

Protocadherin-18b regulates motor axon arborization

As reported previously (Kubota *et al.*, 2008), *pcdh18b* is expressed in neurons of the ventral spinal cord (Figure 1A). Two-color in situ hybridization using riboprobes directed against *pcdh18b* and *isl1* reveals that these ventral neurons are primary motoneurons (Figure 1, B–D). To determine the role of *pcdh18b* in motoneuron development, we designed antisense morpholino oligonucleotides against *pcdh18b* (Figure 2A). Injection of splice-blocking morpholinos into one-cell-stage embryos efficiently blocks the processing of *pcdh18b* transcripts (Figure 2, B and C). The misspliced transcripts are predicted to encode a truncated form of Pcdh18b that lacks the cytoplasmic domain, which was confirmed by cloning and sequencing of the misspliced products (Figure 2D).

To assess the role of Pcdh18b in motoneuron development, we used a transgenic line in which the hb9 promoter drives expression of green fluorescent protein (GFP), *Tg(mnx1:0.6hsp70:GFP)*. In this line, GFP brightly labels primary motoneurons, as well as some secondary motoneurons and other spinal interneurons (Figure 2E). Transgenic embryos were injected with *pcdh18b* morpholinos, and two-photon image stacks of the ventrally projecting CaP axons were collected at 2 d postfertilization (dpf; Figure 2F). Compared to embryos injected with a mismatch control morpholino (*pcdh18b*MOs-1mis), CaP axons from *pcdh18b*MOs1-injected embryos exhibited a dose-dependent decrease in arborization (Figure 2G). Comparable results were obtained with both splice-blocking morpholinos (*pcdh-18b*MOs1 and *pcdh18b*MOs2) and a morpholino targeted to the translational start site (*pcdh18b*MOT). Axons from embryos injected with *pcdh18b*MOs1mis had 39.9 ± 1.9 (mean ± SEM; $n = 24$ axons from eight embryos) total branches, whereas doses of 5 and 10 ng of *pcdh18b*MOs1 resulted in 27.1 ± 1.3 ($n = 60$ axons from 21 embryos, $p = 8e^{-7}$) and 20.3 ± 1.0 ($n = 67$ axons from 24 embryos, $p = e^{-10}$) total branches, respectively. To verify that the effects on motor axon arborization are due to the loss of Pcdh18b, we performed rescue experiments using a bacterial artificial chromosome (BAC) clone that harbors the full *pcdh18b* gene (Figure 3). Compared to BAC-injected embryos (Figure 3A), the total number of axon branches and total branch length were reduced in morphant embryos (Figure 3, B, D, and E). Control embryos exhibited total branch length of 587 ± 14 μm ($n = 66$ axons) and total branch number of 24.9 ± 0.7, compared with 453 ± 12 μm and 20.6 ± 0.7 for morpholino-injected embryos, respectively. These branching defects were rescued in embryos injected both with morpholinos (MOs) and the *pcdh18b* BAC (Figure 3, C–E), which exhibited a total branch length of 549 ± 19 μm ($p = 0.0006$) and total branch number of 24.5 ± 0.8 ($p = 0.003$). To verify that BAC injection rescued Pcdh18b levels, we performed reverse transcription (RT)-PCR on embryos that had been injected with 8 ng of *pcdh18bMOs2* or 8 ng of *pcdh18b-MOs2* and 100 pg of *pcdh18b* BAC DNA (Figure 3F). Coinjected embryos exhibited increased levels of wild-type transcripts.

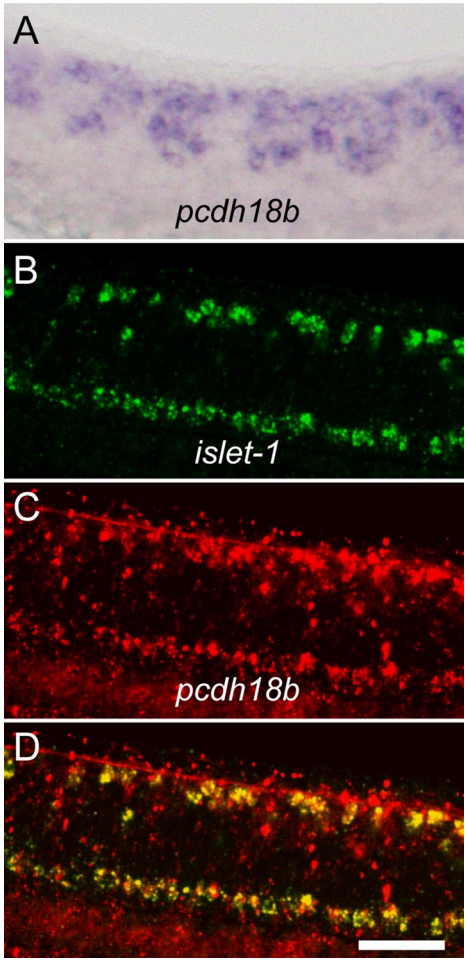

FIGURE 1: Protocadherin-18b is expressed in primary motoneurons. (A) The spinal cord of a 24-h postfertilization (hpf) zebrafish embryo was labeled with riboprobe directed against *pcdh18b*. Both a column of dorsal neurons and serially repeating sets of ventral neurons are labeled. (B) Maximum-intensity projection of two adjacent optical sections labeled by fluorescence in situ hybridization, using a riboprobe directed against *islet-1*, which is a marker of both Rohon–Beard cells (dorsal) and ventral primary motoneurons. Shown is a region of spinal cord from a 24-hpf embryo. (C) Maximum-intensity projection of the same optical sections in B, labeled by fluorescence in situ hybridization with a riboprobe against *pcdh18b*. (D) An overlay of B and C reveals that *pcdh18b* is expressed in dorsal sensory neurons and primary motoneurons. Scale bar, 35 μm.

To determine whether Pcdh18b is required cell autonomously, we performed cell transplantation experiments (Figure 4A). Cells from transgenic embryos were transplanted into wild-type embryos, and GFP-labeled CaP axons were imaged at 2 dpf (Figure 4, B–D). Motor axons of cells transplanted from *pcdh18b*-morphant embryos into wild-type embryos exhibited a decrease in arborization compared with control transplants (Figure 4, B, E, and F). There was a decrease in total branch length (WT → WT, 359.8 ± 34.5, $n = 7$ axons, vs. MO → WT, 239.9 ± 20, $n = 7$ axons; $p = 0.008$) and branch number (WT → WT, 25.6 ± 2.1, vs. MO → WT, 18.5 ± 1.8; $p = 0.009$). In contrast, wild-type cells transplanted into morphant embryos exhibited normal axon arbors (Figure 4, D–F) in both total branch length (316.8 ± 25.4) and total branch number (27.9 ± 2.2). These results indicate that Pcdh18b is required cell autonomously for normal arborization of CaP motor axons and is not required in the adjacent

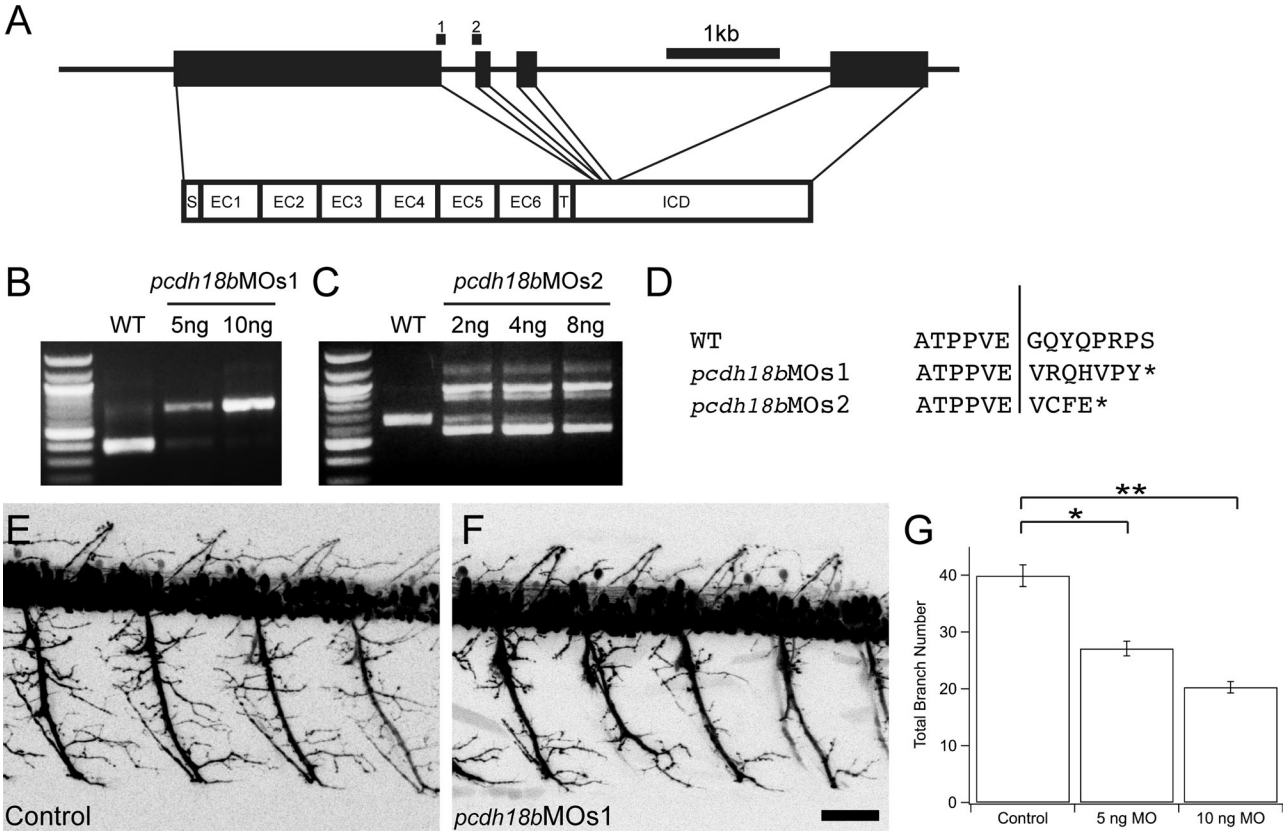

FIGURE 2: Depletion of *pcdh18b* causes defects in motor axon arborization. (A) Schematic diagram showing the genomic organization of *pcdh18b*, as well as the target sites of splice-blocking antisense morpholinos (1, *pcdh18b*MOs1; 2, *pcdh18b*MOs2). EC, ectodomain cadherin repeat; ICD, intracellular domain; S, signal peptide; T, transmembrane domain. (B, C) RT-PCR analysis of embryos injected with *pcdh18b*MOs1 (B) or *pcdh18b*MOs2 (C) reveals efficient knockdown of *pcdh18b*. The increased size of the PCR product reflects the inclusion of intron 1 in transcripts. Targeting of site 2 can result either in loss of exon 2 or inclusion of intron 1. (D) Cloning and sequencing of RT-PCR products from control and morpholino-injected embryos reveals that Pcdh18b is truncated shortly after exon 1. The exon1–exon2 boundary is indicated by a vertical line. (E) Maximum-intensity projection from a two-photon image stack of a live 48-hpf transgenic embryo, *Tg(mnx1:0.6hsp70:GFP)*, which expresses GFP in motor neurons and other spinal interneurons. (F) Maximum-intensity projection of a two-photon image stack of a live 48-hpf transgenic embryo that had been injected with 10 ng of *pcdh18b*MOs1. There is a reduction in motor axon complexity compared with control embryos in E. Scale bar, 25 µm. (G) Analysis of motor axon arbors reveals a dose-dependent loss of branching in embryos injected with *pcdh18b*MOs1. Total branch number: control embryos, 40 ± 1.3 ($n = 23$; mean ± SEM); 5 ng *pcdh18b*MOs1, 27 ± 1.1 (n = 59; $*p = 7 \times 10^{-7}$); 10 ng *pcdh18b*MOs1, 19 ± 0.9 ($n = 66$; $**p = 1.8 \times 10^{-10}$). Significance determined using Wilcoxon signed-rank test.

muscle. This observation is consistent with the fact that *pcdh18b* does not appear to be expressed in muscle (Kubota *et al.*, 2008).

To look more closely at defects in the CaP axon and determine whether synaptogenesis was affected by Pcdh18b loss, we used an *mnx1-3×125bp:Gal4-VP16* expression plasmid to drive transgene expression in single CaP motoneurons (Figure 5). When this plasmid was used to drive GFP expression (Figure 5, A and B), we observed defects in axon branch length (Figure 5C; WT, 491 ± 53.7, vs. *pcdh-18b*MOs2, 291.2 ± 37.3; $p = 0.013$) and branch number (Figure 5D; WT, 28.6 ± 3.0, vs. *pcdh18b*MOs2, 16.1 ± 2.6; $p = 0.014$) similar to those observed in the hb9 transgenic line. To determine defects in presynaptic assembly, we expressed a synaptophysin-GFP (Syp-GFP) fusion protein (Figure 5, E and F), which labels synaptic vesicle clusters. There were fewer Syp-GFP puncta in embryos depleted of Pcdh18b (Figure 5G; WT, 69.5 ± 6.6, vs. *pcdh18b*MOs2, 46.9 ± 2.6; $p = 0.003$), consistent with the reduced extent of the axonal arbor. There was no significant change in the size of Syp-GFP clusters (Figure 5H).

Protocadherin-18b interacts with Nap1

Prior work showed that the cytodomains of both mouse Pcdh10 and chicken Pcdh19 interact directly with Nap1, a core component of the WAVE complex (Nakao *et al.*, 2008; Tai *et al.*, 2010). To determine whether Pcdh18b also interacts with Nap1, we performed coimmunoprecipitation with epitope-tagged Pcdh18b and Nap1 (Figure 6). When cotransfected into HEK293 cells, Nap1-Myc coimmunoprecipitates with full-length Pcdh18b-GFP (Figure 6A). Similarly, Nap1 coimmunoprecipitates with a soluble form of the Pcdh18b intracellular domain (Figure 6B). In contrast, a truncated version of Pcdh18b lacking the intracellular domain (Pcdh18bΔICD) fails to interact with Nap1 (Figure 6C). To determine the relative distributions of Pcdh18b and Nap1 in cells, we cotransfected HEK293 cells with Pcdh18b-GFP and Nap1-Myc (Figure 6, D–F). Nap1-Myc is present diffusely throughout the cytoplasm of transfected cells, including a strong presence in the nucleus and lamellipodia (Figure 6D). Pcdh18b-GFP is present diffusely along the plasma membrane, as well as in discrete puncta

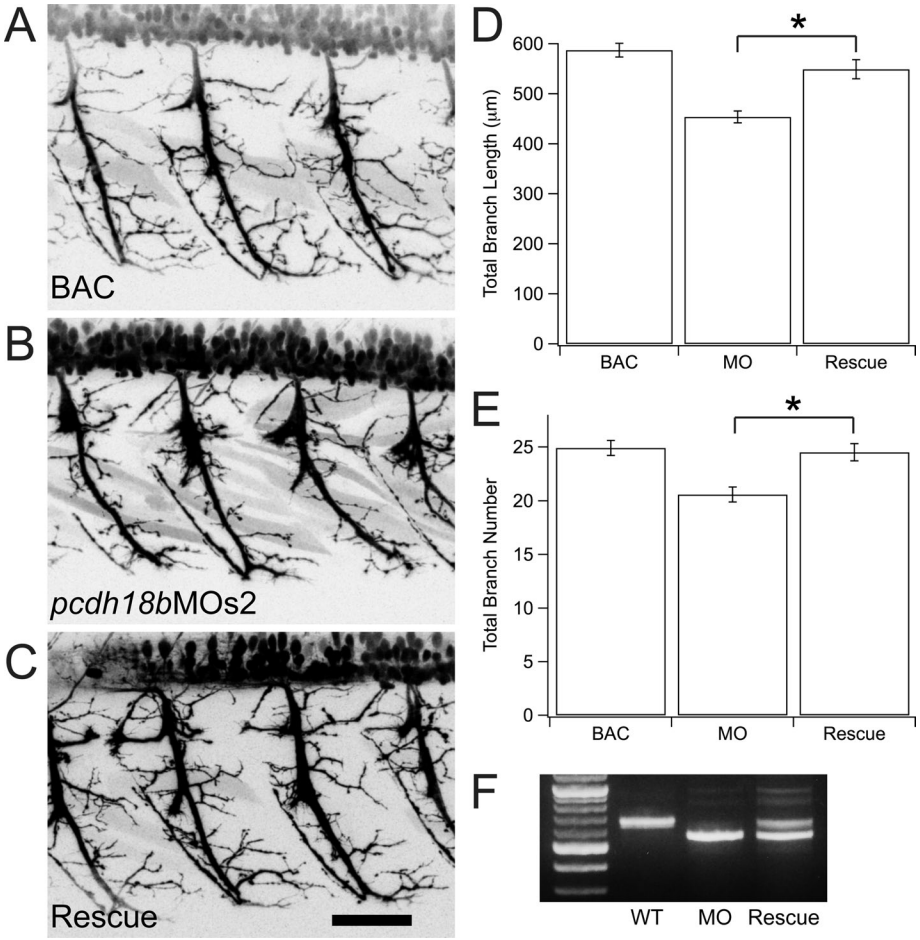

FIGURE 3: Rescue of axon branching defects by injection of *pcdh18b* BAC clone. (A–C) Maximum-intensity projection of a two-photon image stack from *Tg(mnx1:0.6hsp70:GFP)*^{os26} embryos at 48 hpf that were injected with BAC clone CH211-154p8 (A), *pcdh18b*MOs2 (B), or both (C). Scale bar, 25 μm. (D) Injection of BAC CH211-154p8 rescues the defect in total branch length. BAC (587 ± 14 μm, $n = 66$), MO (453 ± 12 μm, $n = 56$), rescue (549 ± 19μm, $n = 71$; *$p = 0.00056$). Significance determined using Wilcoxon signed-rank test. (E) Injection of BAC clone CH211-154p8 also rescues the defect in branch number. BAC, 24.9 ± 0.7; MO, 20.6 ± 0.7; rescue, 24.5 ± 0.8; *$p = 0.0033$. Significance determined using Wilcoxon signed-rank test. (F) Injection of BAC clone CH211-154p8 results in a partial recovery of wild-type *pcdh18b* transcript levels. RT-PCR was performed on wild-type embryos (lane 2), embryos injected with 8 ng of *pcdh18bMOs2* (lane 3), or 8 ng of pcdh18bMOs2 and 100 pg of CH211-154p8 BAC DNA (lane 4).

(Figure 6E). An overlay of Nap1-Myc and Pcdh18b-GFP exhibits extensive overlap of fluorescence signal in the lamellipodia (Figure 6F).

Given that Nap1 is a regulator of actin dynamics and has been shown to participate in neurite outgrowth, we hypothesized that Nap1 could be involved in the axon growth defects exhibited by *pcdh18b* morphants (Figure 7). To test this, we designed morpholinos against *nap1* (Figure 7A). Injection of splice-blocking morpholinos (*nap1*MOs1 or *nap1*MOs2) efficiently impaired the processing of *nap1* transcripts (Figure 7B), resulting in truncated protein (Figure 7C). Injection of a morpholino directed against the translational start site (*nap1*MOT) resulted in a dose-dependent loss of Nap1 (Figure 7D). Depletion of Nap1 using either splice-blocking or translation-blocking morpholinos resulted in axon arborization defects similar to those of *pcdh18b* morphants (Figure 7, E–H). As shown for Pcdh18b, depletion of Nap1 resulted in a loss of total axon branch length (WT, 491 ± 53.7, $n = 7$, vs. *nap1*MOs2, 334.1 ± 28.3, $n = 10$; $p = 0.006$) and branch number (WT, 28.6 ± 3.0, vs. *nap1*MOs2, 17.8 ± 1.3; $p = 0.02$). These results demonstrate that Nap1 participates in the development of CaP motor axons and support the idea that the Pcdh18b–Nap1 interaction could be important for axon development.

Protocadherin-18b and Nap1 control motor axon dynamics

To investigate the effects of Pcdh18b or Nap1 depletion in more detail, we collected in vivo two-photon time-lapse image sequences of GFP-labeled CaP axons (Figure 8, A–C). Growing CaP axons are highly active, exhibiting dynamic filopodia along the axon shaft, as well as the growth cones (Figure 8, A–C). To determine the origins of the branching defects exhibited by *pcdh18b*-and *nap1*-morphant embryos, we quantified the filopodia dynamics in 1-dpf embryos, as the CaP axonal arbor is beginning to elaborate. Compared to control axons, the density of filopodia along the main shaft of the CaP axon was reduced in embryos depleted of either Pcdh18b or Nap1 (Figure 8D; WT, 0.6 ± 0.05 filopodia/μm, $n =$ 8 axons from four embryos, vs. *pcdh18b*-MOs2, 0.47 ± 0.04, $n = 8$ axons from four embryos, $p = 0.002$; vs. *nap1*MOT, 0.42 ± 0.03, $n = 10$ axons from five embryos, $p =$ 0.005). In contrast, loss of neither protein significantly affected the dynamic properties of filopodia, as the lifetimes (Figure 8E), rates of extension and retraction (Figure 8F), and lengths (Figure 8G) were comparable to those of control axons. These data indicate that both Pcdh18b and Nap1 may promote the formation of new filopodia in axons but do not affect the dynamic properties of those filopodia that do form.

DISCUSSION

Accumulating evidence implicates protocadherins in a range of neurodevelopmental disorders, including autism spectrum disorders, schizophrenia, intellectual disability, and epilepsy (Hirano and Takeichi, 2012; Redies *et al.*, 2012). However, the molecular, cellular and developmental functions of protocadherins are poorly understood, as are the pathways linking molecular disruptions to brain disorders. Recently a genomic deletion that includes only the *pcdh18* gene was associated with severe developmental disturbance that included seizures, developmental delay, microcephaly, and behavioral abnormalities, as well as broad morphological defects (Kasnauskiene *et al.*, 2012). A previous study demonstrated a role for a related gene, *pcdh18a,* in cell migration during zebrafish gastrulation (Aamar and Dawid, 2008). However, the neuronal functions of PCDH18 were not previously investigated. Here we demonstrate that Pcdh18b associates with the actin regulator Nap1 and both proteins play a role in the arborization of motor axons in the embryonic zebrafish.

Prior studies implicated protocadherin family members in axon growth. Mice deficient in α-Pcdhs have defects in serotonergic axon tracts (Katori *et al.*, 2009) and exhibit mistargeting of olfactory

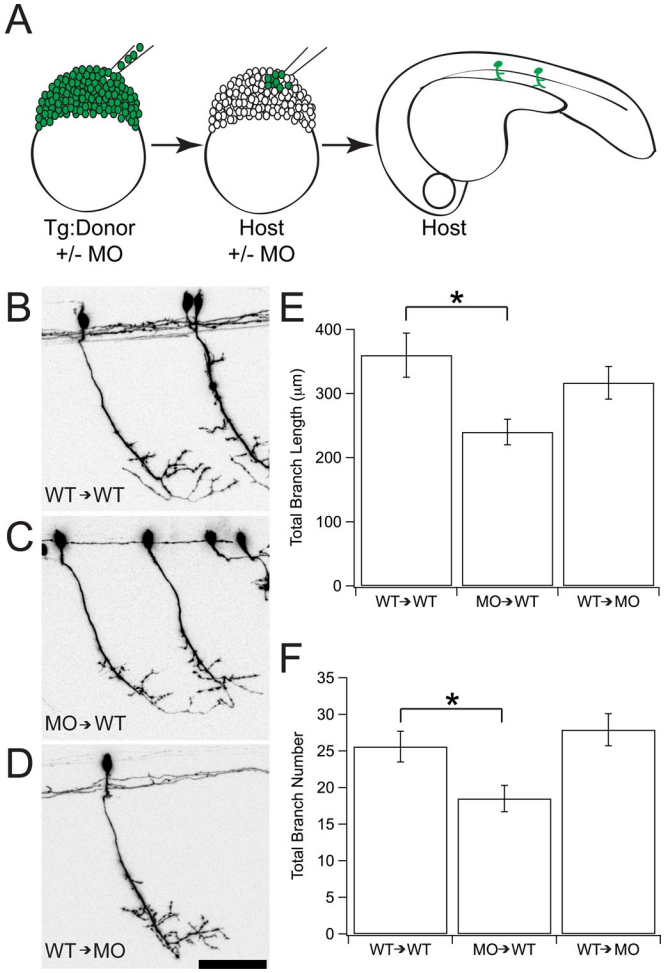

FIGURE 4: Pcdh18b acts cell autonomously in CaP motor axons. (A) Schematic of cell transplantation experiments. Cells are taken from *Tg(mnx1.0:0.6hsp70:GFP)* donor embryos and transplanted into wild-type host embryos. Motoneurons derived from the donor embryos will be fluorescent. Pcdh18b can be knocked down either in the donor or in the host embryos. (B–D) Maximum-intensity projection of a two-photon image stack from 48-hpf host embryos that had been transplanted with cells from *Tg(mnx1:0.6hsp70:GFP)* embryos in which both host and donor embryos were uninjected (B), donor embryos were injected with *pcdh18b*MOs2 (C), or host embryos were injected with *pcdh18b*MOs2 (D). Scale bar, 25 μm. (E) Morphant axons transplanted into a wild-type background exhibited a decrease in total branch length. WT → WT, 359 ± 35μm, $n = 7$; MO → WT, 240 ± 20μm, $n = 7$, $*p = 0.008$; $n = 7$; WT → MO, 317 ± 25μm, $n = 7$. Significance determined using Wilcoxon signed-rank test. (F) Morphant axons transplanted into a wild type background exhibited a decrease in branch number. WT → WT, 25.6 ± 2.1, $n = 7$; MO → WT, 18.5 ± 1.8, $n = 7$, $*p = 0.009$; $n = 7$; WT → MO, 27.9 ± 2.2, $n = 7$, $*p = 0.009$. Significance determined using Wilcoxon signed-rank test.

sensory axons (Hasegawa *et al.*, 2008). Deletion of mouse *pcdh10/OL-pc* causes a defect in thalamocortical tracts in the ventral telencephalon and impairs striatal axon outgrowth in vitro and in vivo (Uemura *et al.*, 2007). Similarly, expression of Pcdh7/NFPC dominant-interfering constructs in *Xenopus* retinal ganglion cells also affects axon outgrowth (Piper *et al.*, 2008). Our results differ in that axon initiation and extension appear to proceed normally. Instead, the branching patterns of CaP axons are sparser, exhibiting fewer branches and reduced total branch length. Time-lapse analysis suggests that the branching defects could be due to a reduced rate in the initiation of filopodia. This could reflect diversity in the specific functions played by different protocadherin family members. It is not clear whether the observed phenotype can be attributed entirely to the loss of Pcdh18b or may reflect a partial dominant-interfering activity of truncated Pcdh18b resulting from the use of splice-blocking morpholinos. However, the robust phenotypic rescue achieved indicates that the full-length protein can largely restore function, even in the presence of truncated Pcdh18b, arguing against a large dominant-interfering effect.

Nap1 is a core component of the WAVE complex, an important regulator of actin dynamics (Bear *et al.*, 1998; Miki *et al.*, 1998; Ismail *et al.*, 2009; Chen *et al.*, 2010). As such, Nap1 and the WAVE complex are ideally situated to regulate axon growth and arborization. Mice lacking Nap1 are defective in neurite outgrowth (Yokota *et al.*, 2007), and Rac1 regulates axon growth through the WAVE complex (Tahirovic *et al.*, 2010). Although it is not known what cell surface interactions or signals lead to the activation or suppression of WAVE-mediated actin dynamics, we show that Nap1 binds to the intracellular domain of Pcdh18b and depletion of either Pcdh18b or Nap1 yields very similar effects on axon branching and dynamics. Pcdh10/OL-pc was previously shown to bind to Nap1 and control contact-dependent cell motility in vitro (Nakao *et al.*, 2008), and chicken Pcdh19 was also shown to interact with Nap1 (Tai *et al.*, 2010). Thus Nap1 and the WAVE complex may be general downstream effectors of δ-Pcdhs. Conversely, the δ-Pcdhs appear to be major regulators of the WAVE complex and actin dynamics during nervous system development.

The interaction of Pcdh10/OL-pc with Nap1 promoted contact-dependent cell motility, suggesting a dependence on homophilic interactions between neighboring cells (Nakao *et al.*, 2008). Our data are consistent with a contact-dependent promotion of filopodia extension, as loss of Pcdh18b or Nap1 reduces the density of filopodia and results in reduced axon arborization. Two observations argue against a homophilic mechanism in the case of Pcdh18b. First, we do not detect expression of *pcdh18b* in the somite, as was shown previously (Kubota *et al.*, 2008). Thus there is no homophilic partner in the tissue adjacent to the extending axons. Second, Pcdh18b functions cell autonomously during the control of CaP axon branching, as wild-type axons transplanted into morphant embryos exhibit normal levels of arborization. It was similarly shown that the role of Pcdh10/OL-pc acts cell autonomously to promote axon outgrowth in striatal neurons and loss of Pcdh10 affects the guidance of axons that do not normally express it (Uemura *et al.*, 2007). These data could be interpreted as evidence either for an indirect role for protocadherins or for heterophilic interactions. Although members of the cadherin superfamily are generally believed to function as calcium-dependent cell adhesion molecules, there is also evidence for diversity in the range of interactions mediated by cadherin superfamily members. Fat and dacshous proteins have been shown to interact heterophilically (Ishiuchi *et al.*, 2009), as have cadherin-23 and protocadherin-15 (Kazmierczak *et al.*, 2007; Sotomayor *et al.*, 2012). Moreover, classic cadherins exhibit heterophilic interactions, with homophilic specificity expressed only as a matter of a quantitative preference (Patel *et al.*, 2006; Katsamba *et al.*, 2009). Thus it is possible that protocadherins participate in both heterophilic and homophilic interactions.

In addition to the defect in axon growth and arborization, we observed a decrease in synaptic vesicle clusters, as represented by puncta of Syp-GFP. It is most likely that the decrease in

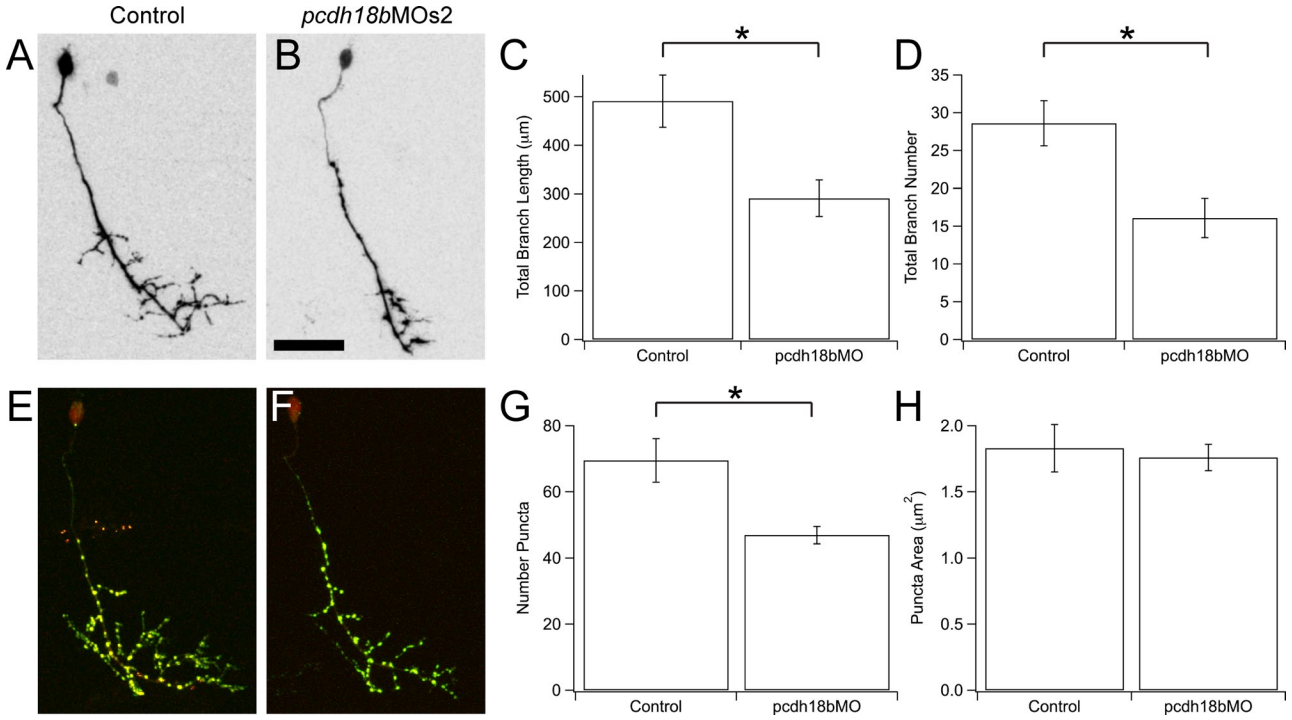

FIGURE 5: Depletion of Pcdh18b results in arborization defects in single, labeled CaP motor axons. (A, B) GFP was expressed in single CaP motoneurons by coinjecting *mnx1-3×125bp:Gal4-VP16* and *14xUAS-E1b:GFP* into control (A) or embryos injected with *pcdh18b*MOs2 (B). Scale bar, 25 μm. (C, D) Coinjection of plasmids with *pcdh18b*MOs2 resulted in decreases in total branch length (C; control, 491 ± 54 μm, $n = 8$; *pcdh18b*MO, 291 ± 37 μm, $n = 10$, $*p = 0.013$) and total branch number (D; control, 28.6 ± 3, $n = 8$; *pcdh18b*MO, 16.1 ± 2.6, $n = 7$, $*p = 0.014$). Significance determined using Wilcoxon signed-rank test. (E, F) Synaptophysin-GFP was coexpressed with Kusabira orange in single CaP motoneurons by coinjecting *mnx1-3×125bp:Gal4-VP16* and *Syp-GFP:KO* into control embryos (A) or embryos injected with *pcdh18b*MOs2 (B). (G) Coinjection of plasmids with *pcdh18b*MOs2 resulted in loss of Syp-GFP puncta (control: 69.5 ± 6.6, $n = 6$; *pcdh18b*MOs2: 46.9 ± 2.6, $n = 26$, $*p = 0.003$). Significance was determined using Wilcoxon signed-rank test. (H) Depletion of Pcdh18b had no effect on the size of Syp-GFP puncta along CaP axonal arbors (control: 1.83 ± 0.18 μm², $n = 6$; *pcdh18b*MOs2: 1.76 ± 0.1 μm²).

putative synapse number is a simple consequence of reduced arbor length, as the density of presynaptic puncta is comparable in control and Pcdh18b-deficient embryos. However, axon arbors exhibit synaptotropic growth (Meyer and Smith, 2006; Ruthazer *et al.*, 2006). It is possible that the reduced extent of arborization could be due to inefficiency in forming or stabilizing synaptic contacts, which would impair the elaboration of a mature arbor. Our time-lapse data indicate that the effect of knocking down either Pcdh18b or Nap1 is not through an effect on synaptotropic growth. The primary effect is a reduction in filopodia density, consistent with a decreased rate in the formation of new filopodia. In contrast, neither the lifetimes of filopodia nor the rates of retraction are significantly affected. Given that previous time-lapse studies showed that new axon branches form from the stabilization and engorgement of filopodia, we expect that any role of Pcdh18b in stabilizing filopodia through adhesive contacts would manifest as an effect on filopodia lifetimes. It is interesting to note that despite the sizable differences in CaP axonal arbors at ~48 hpf, the effects on axon dynamics at ~24 hpf are relatively modest. It is possible that small quantitative changes in dynamics (e.g., a reduced rate of initiating filopodia) could have cumulative effects, leading to more pronounced consequences later in development. This could be important in understanding the relationship of molecular perturbations to the etiology of neurodevelopmental disorders.

MATERIALS AND METHODS

Fish maintenance

Adult zebrafish (*Danio rerio*) and embryos of the Tübingen longfin and AB strains or *Tg(mnx1:0.6hsp70:GFP)os26* (Hao le *et al.*, 2012) were maintained at ~28.5°C and staged according to *The Zebrafish Book* (Westerfield, 1995). Embryos were raised in E3 embryo medium (Westerfield, 1995) with 0.003% phenylthiourea (Sigma-Aldrich, St. Louis, MO) to inhibit pigment formation. Larvae were anesthetized in 0.016% ethyl 3-amino benzoate methanesulfonate (Sigma-Aldrich). All procedures were carried out in accordance with Institutional Animal Care and Use Committee–approved protocols.

Whole-mount in situ hybridization

The constant cytoplasmic domain of *pcdh18b* was cloned by RT-PCR. A T7 RNA polymerase binding site was added to the antisense strand by PCR. This PCR product was used as template for in vitro transcription (Promega, Madison, WI). Antisense riboprobe was labeled with digoxigenin-dUTP (Roche, Indianapolis, IN). Embryos were fixed at 4°C overnight in 4% paraformaldehyde in phosphate-buffered saline (PBS), dehydrated in 25, 50, 75% methanol, and stored in 100% methanol overnight at –20°C. They were rehydrated in decreasing concentrations of methanol and permeabilized using proteinase K (10 μg/ml; Roche). Embryos were refixed in 4% paraformaldehyde before hybridization. Digoxigenin-dUTP–labeled riboprobe was added to the final concentration of 200 ng/ml, and

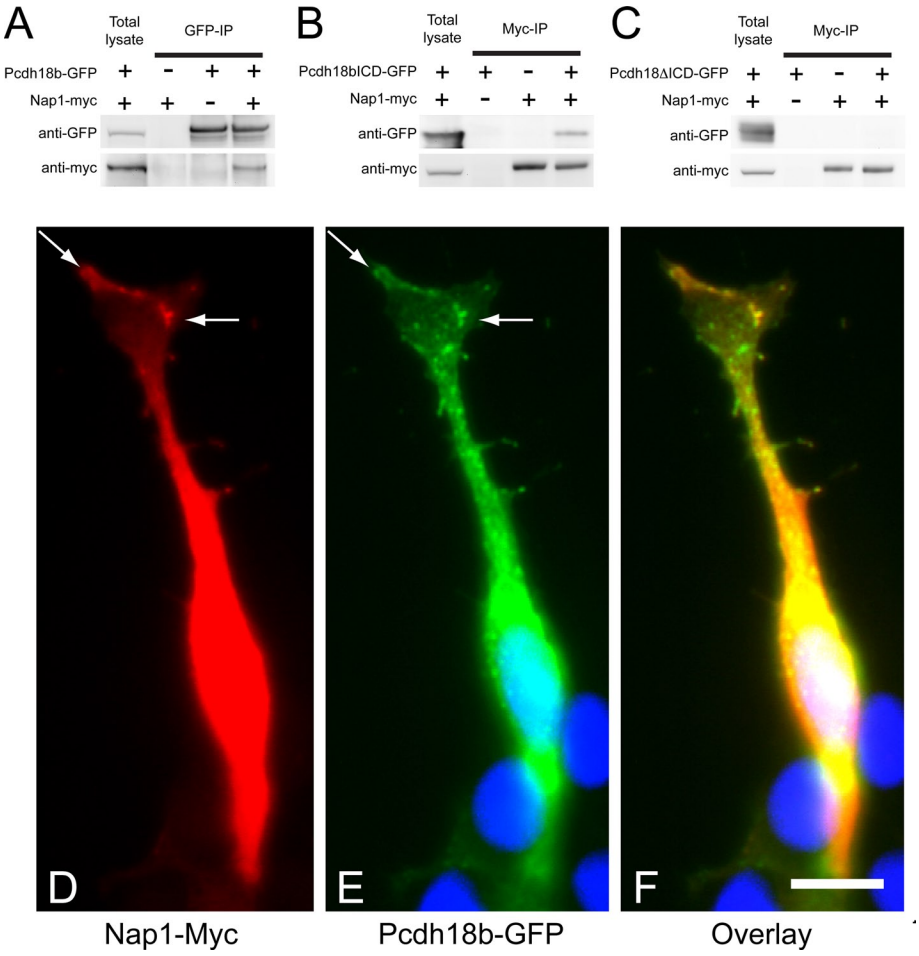

FIGURE 6: Interaction of Pcdh18b with Nap1. (A) When cotransfected into HEK293 cells, Nap1-myc coimmunoprecipitates with Pcdh18b-GFP. (B) Nap1-myc coimmunoprecipitates with the intracellular domain of Pcdh18b (Pcdh18bICD-GFP). (C) Nap1-myc does not coimmunoprecipitate with a truncated form of Pcdh18b that lacks the intracellular domain (Pcdh18bΔICD-GFP). (D–F) Nap1-Myc (D) and Pcdh18b-GFP (E) were cotransfected into HEK293 cells. Nap1-Myc colocalized with Pcdh18b-GFP along the membrane of lamellipodia (F). Scale bar, 10 μm.

hybridization was carried out at 65°C overnight. Alkaline phosphatase–conjugated anti-digoxigenin Fab fragments (Roche) were used at 1:5000 dilution. Nitro blue tetrazolium/5-bromo-4-chloro-3′-indolyphosphate (Roche) was used for the coloration reaction. Transmitted light images were captured on a Leica MZ16F stereomicroscope (Leica Microsystems, Buffalo Grove, IL). For two-color in situ hybridization, commercially available TSA Kit (Invitrogen, Carlsbad, CA) was used to visualize digoxigenin-labeled *pcdh18b* riboprobe and fluorescein-labeled *islet1* riboprobes. The two-color fluorescent in situs were collected on a custom-built two-photon microscope. The Ti:sapphire laser (Coherent, Santa Clara, CA) was tuned to 740 nm, and a Zeiss 20×/numerical aperture (NA) 0.5 water immersion objective was used. Image stacks were collected at 2-μm spacing.

Plasmids, BACs, and DNA injections

To drive transgene expression in individual CaP motoneurons, we used either of two Gal4-VP16 driver plasmids. The first was ~8 kb of genomic sequence upstream of the start codon of the *neuropilin-1a* gene, *nrp1a:Gal4-VP16*. The second was *mnx1-3×125bp:Gal4-VP16* (Zelenchuk and Bruses, 2011). These were injected into one-cell-stage embryos at a concentration of ~25 ng/μl. To express GFP, we coinjected 25 ng/μl 5xUAS:GFP with one of the Gal4 driver plasmids. For the synaptophysin-GFP experiments, we used a double-headed UAS plasmid to coexpress synaptophysin-GFP with Kusabira orange (*pDual:Syp-GFP:KO*).

For zebrafish *pcdh18b* constructs, PCR primers were used to amplify the *pcdh18b* coding sequence. The 5′ primer contained a *Eco*RI restriction site and a Kozak sequence, and the 3′ primer removed the stop codon and included codons for three glycine residues and a *Bam*HI restriction site that placed *pcdh18b* in-frame with the N1 reading frame of Clontech vectors. This fragment was then subcloned into pEGFP-N1. The Pcdh18b-GFP fusion was sequenced and used as PCR template to generate both Pcdh18bΔICD-GFP and Pcdh18bICD-GFP.

To clone zebrafish *nap1*, PCR primers were designed against a *nap1* sequence identified in a BLAST search. The 5′ primer contained a *Kpn*I restriction site and a Kozak sequence, and the 3′ primer removed the stop codon and included codons for three glycine residues and an *Age*I restriction site that placed *nap1* in-frame with the N1 reading frame of Clontech vectors. The *nap1* fragment was then subcloned into a CMV:Myc-N1 vector.

The *pcdh18b* gene comprises four protein-encoding exons spread over ~8 kb. The entire *pcdh18b* gene is contained on the BAC clone, CH211-154p8. To facilitate broad expression, we used homologous recombination to insert the inverted Tol2 recognition arms (iTol2 cassette) into the BAC clone backbone. For the rescue experiments, 2 nl of 100 ng/μl pure BAC DNA was coinjected with 100 ng/μl mRNA encoding the Tol2 transposase.

Imaging and analysis

Labeled embryos were embedded in 1% agarose and imaged on a custom-built two-photon microscope. Excitation was provided by a Ti:sapphire laser tuned to 910 nm. For analysis of axonal arbors at 2 dpf, fluorescently labeled CaP motoneurons were imaged with a 20×/0.5 NA objective (pixel size, 0.4 μm). Image stacks of up to 30 optical sections were collected at 1.5-μm intervals. Individual sections were gamma adjusted (0.6), filtered (Gaussian blur, radius 0.7 pixel), and used to produce a maximum-intensity projection. Tracing and analysis of CaP axon arbors was performed in Fiji (Schindelin *et al.*, 2012), using the Simple Neurite Tracer plug-in (Longair *et al.*, 2011). Complete CaP axonal arbors were traced through three-dimensional image stacks. The sum of length of all the branches and total number of branch tips for each CaP axons were measured. Quantification of synaptic puncta was performed on unprocessed images using Fiji. A polygonal selection encompassing the branched region of the axon was made. The region within the polygonal selection was thresholded, and the number and size of puncta was determined using the Analyze particles command. The size of puncta was approximated as the area of

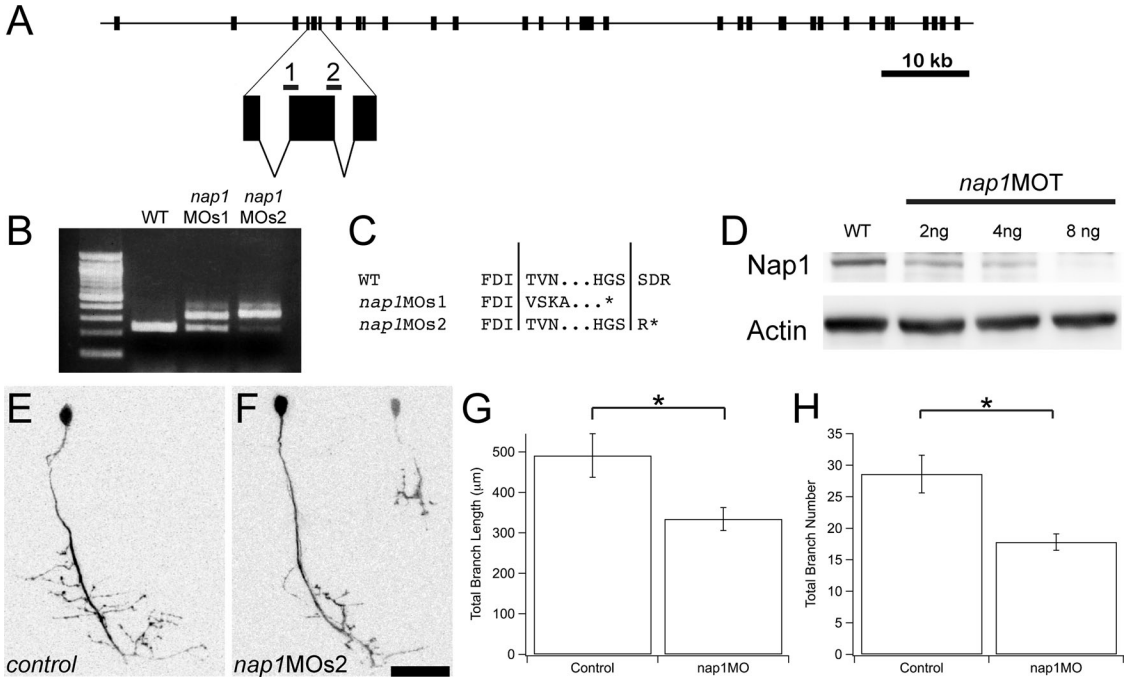

FIGURE 7: Depletion of Nap1 results in axon arborization defects. (A) Schematic diagram showing the genomic organization of *nap1*, as well as the target sites of splice-blocking antisense morpholinos (1, *nap1*MOs1; 2, *nap1*MOs2). (B) RT-PCR analysis of embryos injected with *nap1*MOs1 or *nap1*MOs2 reveals efficient knockdown of *nap1*. The increased size of the PCR product reflects the inclusion of an intron in transcripts. (C) Cloning and sequencing of RT-PCR products from control and morpholino-injected embryos reveals that Nap1 is truncated due to a premature stop codon. The exon–exon boundaries are indicated by the vertical lines. (D) Western blot showing dose-dependent knockdown of Nap1 using a translation-blocking morpholino. (E,F) GFP was expressed in single CaP motoneurons by coinjecting *mnx1-3×125bp:Gal4-VP16* and *14xUAS-E1b:GFP* into control (E) or *nap1MOs2*-morphant embryos (F). (G, H) Depletion of Nap1 resulted in significant decrease in both branch length (G; control: 491 ± 54, $n = 7$; *nap1*MO: 334 ± 28, $n = 10$, $^*p = 0.006$) and branch number (H; control: 28.6 ± 3, $n = 7$; *nap1*MO: 17.8 ± 1.3, $n = 10$, $^*p = 0.02$).

detected particles in pixels. Identical thresholds were used for all data sets.

For time-lapse analysis of filopodia dynamics, labeled CaP axons were imaged with a Zeiss 40×/0.8 NA objective (pixel size, 0.167 µm). Image stacks consisting of 13 optical sections at 1.5-µm spacing were collected at 1-min intervals for 1 h. The highest-quality time-lapse sequences were selected for filopodia analysis. Fiji was used to measure the lengths of filopodia in each frame of each time-lapse sequence. The resulting values were exported into Matlab, and quantitative data were extracted using custom scripts. Lengths were defined as the distance from the base of the filopodium to its tip in maximum-intensity projections. The rate of extension/retraction for a given filopodium was defined as the change in length between successive frames. Filopodia extension/retraction rates for a given motor neuron were calculated as the mean rate of extension or retraction for all filopodia observed on that neuron; these rates were averaged for four axons present in four separate embryos for both control and morphant embryos. The lifetime of an individual filopodium was defined as length of time for which its length was measurable. A filopodium extending from a position at which one had previously disappeared was counted as a second filopodium. The average filopodium lifetime was calculated for each axon, and these numbers were averaged for four axons from four control or morphant embryos. Filopodia density was calculated as the number of filopodia per unit length measured from the first time point from each of eight time-lapse sequences for control and morphant embryos. Statistical significance was determined in IGOR Pro (Wavemetrics, Lake Oswego, OR) using the Wilcoxon signed-rank test. Differences were deemed significant for $p < 0.05$.

Coimmunoprecipitation, Western blotting, and immunocytochemistry

Human embryonic kidney (HEK293) cells were maintained in DMEM supplemented with 10% fetal bovine serum and penicillin/streptomycin at 37°C with 5% CO_2. HEK293 cells were transfected with plasmids encoding Nap1-Myc and Pcdh18b-GFP, Pcdh18bΔICD-GFP, or Pcdh18bICD-GFP using calcium phosphate precipitation. After 24 h, cells were scraped into PBS, pelleted, lysed on ice in cell lysis buffer (CLB; 20 mM Tris, pH 7.5, 150 mM NaCl, 1 mM $CaCl_2$, 0.5% Triton X-100, 1 mM phenylmethylsulfonyl fluoride, Complete Protease Inhibitor Cocktail [Roche]), and microcentrifuged at 4°C for 10 min. Supernatants were incubated with 2 mg of anti-GFP (Invitrogen) or anti-Myc (Sigma) primary antibody for 2 h at 4°C before the addition of protein A–Sepharose (GE Healthcare, Piscataway, NJ), and the coimmunoprecipitation was allowed to incubate overnight at 4°C. The beads were washed five times in CLB, resuspended in loading buffer, and boiled for 5 min. Samples were loaded onto 10% Bis-Tris NuPAGE gels (Invitrogen) and subjected to electrophoresis. Proteins were then transferred (Bio-Rad, Hercules, CA) to nitrocellulose (GE Healthcare), blocked with 5% nonfat milk in Tris-buffered saline/Tween 20, and incubated overnight with primary antibody (anti-GFP, 1:1000; anti-Myc, 1:5000). Horseradish peroxidase–conjugated secondary antibodies (Jackson ImmunoResearch, West Grove, PA) were used at 1:5000, and the chemiluminescence signal was amplified using

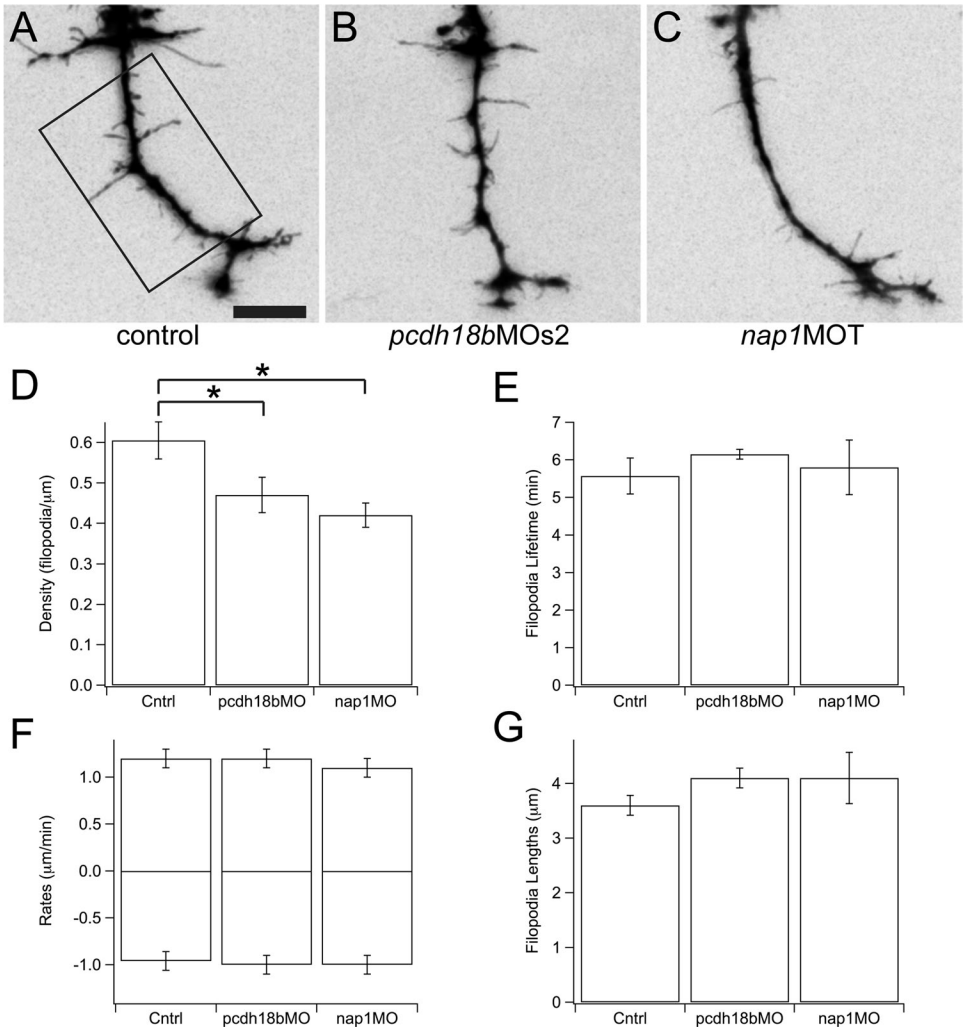

FIGURE 8: Analysis of filopodia dynamics in 1-dpf embryos. (A–C) Frames from time-lapse image sequences of GFP-labeled axons from a control embryo (A) or embryos injected with *pcdh18b*MOs2 (B) or *nap1*MOT (C). Analysis of filopodia dynamics was performed on the axon shaft of the ventrally projecting CaP motor axon (boxed region in A). Scale bar, 10 μm. (D) Density of filopodia along CaP axon shaft. The number of filopodia per micrometer axon was measured for control embryos (0.6 ± 0.05 filopodia/μm, $n = 8$) and embryos injected with morpholinos against *pcdh18b*MOs2 (0.47 ± 0.04 filopodia/μm, $n = 8$) or *nap1*MOT (0.42 ± 0.04 filopodia/μm, $n = 10$). Knockdown of Pcdh18b or Nap1 results in a decrease of filopodia (*pcdh18b*MO, $*p = 0.002$; *nap1*MO, $*p = 0.005$; Wilcoxon signed-rank test). (E) The lifetimes of filopodia were not affected by depletion of either Pcdh18b or Nap1. (F) The rates of extension (positive rates) and retraction (negative rates) for filopodia were measured. There was no discernible effect on the rate of filopodia extension or retraction due to depletion of Pcdh18b or Nap1. (G) The maximal length obtained by each filopodium was measured. The depletion of neither Pcdh18b nor Nap1 had a significant effect on the lengths of filopodia.

Western Lightning Ultra (Perkin Elmer, Waltham, MA). Blots were imaged on an Omega 12iC Molecular Imaging System (UltraLum).

To localize Pcdh18b and Nap1 in HEK293 cells, we transfected cells with Pcdh18b-GFP and Nap1-Myc plasmids. Transfections were performed using Lipofectamine 2000 and carried out according to the manufacturer's instructions (Invitrogen). After 24 h, cells were fixed in 4% paraformaldehyde in PBS, permeabilized in PBS plus 0.25% Triton X-100, and blocked in PBS plus 3% bovine serum albumin plus 2% normal goat serum. The anti-Myc antibody (Sigma) was used at a dilution of 1:250 in block solution, and a DyLight 549–conjugated secondary antibody (Jackson ImmunoResearch) was used at 1:500. Coverslips were mounted in Fluoromount G (Electron Microscopy Sciences, Hatfield, PA) and imaged on a Zeiss Axiostar microscope (Carl Zeiss Microimaging, Thornwood, NY).

Transplantation

To aid in visualization, we used *Tg(hb9-hsp70:gfp)* embryos with GFP-labeled motor neurons as donors and ABLF embryos as host. To ensure correct positioning of the labeled ectopic motor neurons into host embryos, we carried out gastrula-stage transplantation at 50% epiboly with the help of previously characterized fate map (Kimmel *et al.*, 1990). The procedure was followed according to a published protocol (Deschene and Barresi, 2009).

Morpholino and DNA injections

Antisense morpholino oligonucleotides were purchased from GeneTools. The morpholinos were dissolved in dH_2O at ~8 ng/nl, aliquoted, and stored at –80°C. For use, morpholinos were diluted to a working concentration of 2–8 ng/nl in dH_2O, and 1–2 nl was

injected into one-cell-stage embryos. The morpholinos used in this study are as follows:

pcdh18b-MOT:	5′-AGTTGTTCCCATATTTGAAGACGTG-3′
pcdh18b-MOs1:	5′-AACGTGTTGTCTTACCTCGACTGGT-3′
pcdh18b-MOs1mis:	5′-AAgGTcTTGTCTTAgCTCcACTcGT-3′
pcdh18b-MOs2:	5′-GTGATTGGTTACCTGTAGCTCCTGG-3′
nap1-MOT:	5′-CCGAGACATGGCTCAAACGAC-CGTC-3′
nap1-MOT-mis:	5′-CCcAGACATcGCTCAAACcACCcTC-3′
nap1-MOs1:	5′-GGTCAAAATTTACAGTCTGCATTGT-3′
nap1-MOs2:	5′-ACTATGCATTACCTTGAACCGTGTG-3′

The following amounts were used in this study: *pcdh18b*-MOT, 8 ng; *pcdh18b*-MOS1, 10 ng; *pcdh18b*-MOS2, *nap1*-MOS1, 4 ng; *nap1*-MOS2, 8 ng; *nap1*-MOT, 8 ng. Control morpholinos were injected at 8 ng.

For rescue experiments, we used the BAC clone CH211-154p8, which harbors the complete *pcdh18b* gene. In addition, we inserted an iTol2 cassette to facilitate genome insertion and expression (Suster *et al.*, 2011). Purified BAC DNA was used at 100 ng/μl and coinjected with 100 pg of mRNA encoding Tol2 transposase.

ACKNOWLEDGMENTS

This work was partially supported by National Science Foundation/American Recovery and Reinvestment Act Grant IOS 0920357 and National Institutes of Health Grant 1R21MH099453 to J.D.J and Neurosciences Core Grant P30 NS045758. We thank Juan Bruses for the *3×125bp-mnx:Gal4-VP16* plasmid.

REFERENCES

Aamar E, Dawid IB (2008). Protocadherin-18a has a role in cell adhesion, behavior and migration in zebrafish development. Dev Biol 318, 335–346.

Bear JE, Rawls JF, Saxe CL 3rd (1998). SCAR, a WASP-related protein, isolated as a suppressor of receptor defects in late *Dictyostelium* development. J Cell Biol 142, 1325–1335.

Biswas S, Emond MR, Jontes JD (2010). Protocadherin-19 and N-cadherin interact to control cell movements during anterior neurulation. J Cell Biol 191, 1029–1041.

Chen Z, Borek D, Padrick SB, Gomez TS, Metlagel Z, Ismail AM, Umetani J, Billadeau DD, Otwinowski Z, Rosen MK (2010). Structure and control of the actin regulatory WAVE complex. Nature 468, 533–538.

Deschene ER, Barresi MJ (2009). Tissue targeted embryonic chimeras: zebrafish gastrula cell transplantation. J Vis Exp 31, 1422.

Eisen JS, Myers PZ, Westerfield M (1986). Pathway selection by growth cones of identified motoneurones in live zebra fish embryos. Nature 320, 269–271.

Emond MR, Biswas S, Jontes JD (2009). Protocadherin-19 is essential for early steps in brain morphogenesis. Dev Biol 334, 72–83.

Hao le T, Wolman M, Granato M, Beattie CE (2012). Survival motor neuron affects plastin 3 protein levels leading to motor defects. J Neurosci 32, 5074–5084.

Hasegawa S, Hamada S, Kumode Y, Esumi S, Katori S, Fukuda E, Uchiyama Y, Hirabayashi T, Mombaerts P, Yagi T (2008). The protocadherin-alpha family is involved in axonal coalescence of olfactory sensory neurons into glomeruli of the olfactory bulb in mouse. Mol Cell Neurosci 38, 66–79.

Hirano S, Takeichi M (2012). Cadherins in brain morphogenesis and wiring. Physiol Rev 92, 597–634.

Hulpiau P, van Roy F (2009). Molecular evolution of the cadherin superfamily. Int J Biochem Cell Biol 41, 349–369.

Hulpiau P, van Roy F (2011). New insights into the evolution of metazoan cadherins. Mol Biol Evol 28, 647–657.

Ishiuchi T, Misaki K, Yonemura S, Takeichi M, Tanoue T (2009). Mammalian fat and dachsous cadherins regulate apical membrane organization in the embryonic cerebral cortex. J Cell Biol 185, 959–967.

Ismail AM, Padrick SB, Chen B, Umetani J, Rosen MK (2009). The WAVE regulatory complex is inhibited. Nat Struct Mol Biol 16, 561–563.

Kasnauskiene J, Ciuladaite Z, Preiksaitiene E, Matuleviciene A, Alexandrou A, Koumbaris G, Sismani C, Pepalyte I, Patsalis PC, Kucinskas V (2012). A single gene deletion on 4q28.3: PCDH18—a new candidate gene for intellectual disability? Eur J Med Gen 55, 274–277.

Katori S, Hamada S, Noguchi Y, Fukuda E, Yamamoto T, Yamamoto H, Hasegawa S, Yagi T (2009). Protocadherin-alpha family is required for serotonergic projections to appropriately innervate target brain areas. J Neurosci 29, 9137–9147.

Katsamba P *et al.* (2009). Linking molecular affinity and cellular specificity in cadherin-mediated adhesion. Proc Natl Acad Sci USA 106, 11594–11599.

Kazmierczak P, Sakaguchi H, Tokita J, Wilson-Kubalek EM, Milligan RA, Muller U, Kachar B (2007). Cadherin 23 and protocadherin 15 interact to form tip-link filaments in sensory hair cells. Nature 449, 87–91.

Kim SH, Yamamoto A, Bouwmeester T, Agius E, Robertis EM (1998). The role of paraxial protocadherin in selective adhesion and cell movements of the mesoderm during *Xenopus* gastrulation. Development 125, 4681–4690.

Kimmel CB, Warga RM, Schilling TF (1990). Origin and organization of the zebrafish fate map. Development 108, 581–594.

Kubota F, Murakami T, Tajika Y, Yorifuji H (2008). Expression of protocadherin 18 in the CNS and pharyngeal arches of zebrafish embryos. Int J Dev Biol 52, 397–405.

Leung LC, Urbancic V, Baudet ML, Dwivedy A, Bayley TG, Lee AC, Harris WA, Holt CE (2013). Coupling of NF-protocadherin signaling to axon guidance by cue-induced translation. Nat Neurosci 16, 166–173.

Longair MH, Baker DA, Armstrong JD (2011). Simple Neurite Tracer: open source software for reconstruction, visualization and analysis of neuronal processes. Bioinformatics 27, 2453–2454.

Meyer MP, Smith SJ (2006). Evidence from in vivo imaging that synaptogenesis guides the growth and branching of axonal arbors by two distinct mechanisms. J Neurosci 26, 3604–3614.

Miki H, Suetsugu S, Takenawa T (1998). WAVE, a novel WASP-family protein involved in actin reorganization induced by Rac. EMBO J 17, 6932–6941.

Myers PZ (1985). Spinal motoneurons of the larval zebrafish. J Comp Neurol 236, 555–561.

Myers PZ, Eisen JS, Westerfield M (1986). Development and axonal outgrowth of identified motoneurons in the zebrafish. J Neurosci 6, 2278–2289.

Nakao S, Platek A, Hirano S, Takeichi M (2008). Contact-dependent promotion of cell migration by the OL-protocadherin-Nap1 interaction. J Cell Biol 182, 395–410.

Nollet F, Kools P, van Roy F (2000). Phylogenetic analysis of the cadherin superfamily allows identification of six major subfamilies besides several solitary members. J Mol Biol 299, 551–572.

Patel SD *et al.* (2006). Type II cadherin ectodomain structures: implications for classical cadherin specificity. Cell 124, 1255–1268.

Piper M, Dwivedy A, Leung L, Bradley RS, Holt CE (2008). NF-protocadherin and TAF1 regulate retinal axon initiation and elongation in vivo. J Neurosci 28, 100–105.

Redies C, Hertel N, Hubner CA (2012). Cadherins and neuropsychiatric disorders. Brain Res 1470, 130–144.

Ruthazer ES, Li J, Cline HT (2006). Stabilization of axon branch dynamics by synaptic maturation. J Neurosci 26, 3594–3603.

Schindelin J *et al.* (2012). Fiji: an open-source platform for biological-image analysis. Nature methods 9, 676–682.

Sotomayor M, Weihofen WA, Gaudet R, Corey DP (2012). Structure of a force-conveying cadherin bond essential for inner-ear mechanotransduction. Nature 492, 128–132.

Suster ML, Abe G, Schouw A, Kawakami K (2011). Transposon-mediated BAC transgenesis in zebrafish. Nat Protoc 6, 1998–2021.

Tahirovic S, Hellal F, Neukirchen D, Hindges R, Garvalov BK, Flynn KC, Stradal TE, Chrostek-Grashoff A, Brakebusch C, Bradke F (2010). Rac1 regulates neuronal polarization through the WAVE complex. J Neurosci 30, 6930–6943.

Tai K, Kubota M, Shiono K, Tokutsu H, Suzuki ST (2010). Adhesion properties and retinofugal expression of chicken protocadherin-19. Brain Res 1344, 13–24.

Uemura M, Nakao S, Suzuki ST, Takeichi M, Hirano S (2007). OL-Protocadherin is essential for growth of striatal axons and thalamocortical projections. Nat Neurosci 10, 1151–1159.

Westerfield M (1995). The Zebrafish Book Eugene: University of Oregon Press.

Yokota Y, Ring C, Cheung R, Pevny L, Anton ES (2007). Nap1-regulated neuronal cytoskeletal dynamics is essential for the final differentiation of neurons in cerebral cortex. Neuron 54, 429–445.

Zelenchuk TA, Bruses JL (2011). In vivo labeling of zebrafish motor neurons using an mnx1 enhancer and Gal4/UAS. Genesis 49, 546–554.